AD-A150 001 THE VALENCE- AND CONDUCTION-BAND STRUCTURE OF THE SAPPHIRE (1102) SURFACE(U) CALIFORNIA UNIV LOS ANGELES DEPT OF CHEMISTRY AND BIOCHEMISTR.. W J GIGNAC ET AL. 1/1

UNCLASSIFIED DEC 84 TR-4 N00014-83-K-0612 F/G 20/2 NL

END

DATE FILMED

3-85

DTIC

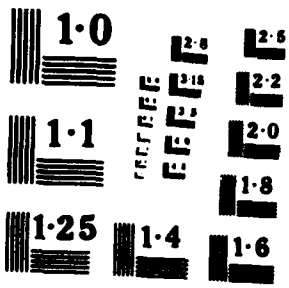
1·0
2·8
2·5
2·2
1·1
2·0
1·8
1·25
1·4
1·6

UNCLASSIFIED

SECURITY CLASSIFICATION OF THIS PAGE (When Data Entered)

REPORT DOCUMENTATION PAGE

READ INSTRUCTIONS BEFORE COMPLETING FORM

1 REPORT NUMBER: 4

2 GOVT ACCESSION NO.:

3 RECIPIENT'S CATALOG NUMBER:

4 TITLE (and Subtitle): The Valence- and Conduction-Band Structure of the Sapphire ($1\bar{1}02$) Surface.

5 TYPE OF REPORT & PERIOD COVERED: Technical Report

6 PERFORMING ORG. REPORT NUMBER:

7 AUTHOR(s): W.J. Gignac, R. Stanley Williams, and S.P. Kowalczyk

8 CONTRACT OR GRANT NUMBER(s): N00014-83-K-0612

9 PERFORMING ORGANIZATION NAME AND ADDRESS: Department of Chemistry & Biochemistry, U C L A - Los Angeles, CA 90024

10 PROGRAM ELEMENT, PROJECT, TASK AREA & WORK UNIT NUMBERS:

11 CONTROLLING OFFICE NAME AND ADDRESS: Chemistry Program Office, Office of Naval Research, Arlington VA, 22217

12 REPORT DATE: December 1984

13 NUMBER OF PAGES: 48

14 MONITORING AGENCY NAME & ADDRESS (if different from Controlling Office):

15 SECURITY CLASS (of this report): UNCLASSIFIED

15a DECLASSIFICATION DOWNGRADING SCHEDULE:

16 DISTRIBUTION STATEMENT (of this Report): Approved for public release; distribution unlimited

17 DISTRIBUTION STATEMENT (of the abstract entered in Block 20, if different from Report):

18 SUPPLEMENTARY NOTES: To be published in Physical Review B

19 KEY WORDS (Continue on reverse side if necessary and identify by block number): Sapphire - Aluminum Oxide - X-ray photoemission - electron energy loss - plasmon - surface state - density-of-states.

20 ABSTRACT (Continue on reverse side if necessary and identify by block number):

X-ray photoelectron and electron energy-loss spectroscopies have been employed to investigate the valence- and conduction-band densities-of-states of the sapphire ($1\bar{1}02$) surface. The photoemission spectrum of the valence-band region has been adjusted to remove cross-section effects and compared to the recent theoretical density-of-states calculated by Ciraci and Batra. The energy-loss data have been used to determine the bulk plasmon energy of sapphire, 24.0 ± .3 eV, as well as the locations of 8 regions of high conduction-band state density within 20 eV above the conduction-band minimum. One of these regions is an empty /OVER

DD FORM 1 JAN 73 1473 EDITION OF 1 NOV 65 IS OBSOLETE

S/N 0102-LF-014-6601

UNCLASSIFIED

SECURITY CLASSIFICATION OF THIS PAGE (When Data Entered)

AD-A150 001

DTIC FILE COPY

DTIC ELECTE FEB 08 1985 S D E

84 12 17 002

DISCLAIMER NOTICE

THIS DOCUMENT IS BEST QUALITY PRACTICABLE. THE COPY FURNISHED TO DTIC CONTAINED A SIGNIFICANT NUMBER OF PAGES WHICH DO NOT REPRODUCE LEGIBLY.

Copy available to DTIC does not
permit fully legible reproduction

Accession For
NTIS GRA&I ☒
DTIC TAB ☐
Unannounced ☐
Justification
By
Distribution/
Availability Codes
Dist | Avail and/or Special
A-1 | 23 CAT

OFFICE OF NAVAL RESEARCH

Research Contract N00014-83-K-0612

TECHNICAL REPORT No. 4

THE VALENCE- AND CONDUCTION-BAND STRUCTURE OF THE SAPPHIRE ($1\bar{1}01$) SURFACE.

by

W.J. Gignac, R. Stanley Williams, and S.P. Kowalczyk

Prepared for Publication

in

Physical Review B

Department of Chemistry and Biochemistry
University of California, Los Angeles, CA 90024

December, 1984

Reproduction in whole or part is permitted for
any purpose of the United States Government.

This document has been approved for public release and sale;
its distribution is unlimited.

The Valence- and Conduction-Band Structure of the Sapphire (1$\bar{1}$02) Surface

W.J. Gignac* and R.Stanley Williams

Department of Chemistry and Biochemistry
University of California Los Angeles
Los Angeles, California 90024

and

Steven P. Kowalczyk

Rockwell International Corporation
Microelectronics Research and Development Center
Thousand Oaks, California 91360

*Present Address: Hughes Research Laboratories, 3011 Malibu Canyon Rd., Malibu, Ca. 90265.

+ or -

ABSTRACT

X-ray photoelectron and electron energy loss spectroscopies have been employed to investigate the valence- and conduction-band densities-of-states of the sapphire ($1\bar{1}02$) surface. The photoemission spectrum of the valence-band region has been adjusted to remove cross-section effects and compared to the recent theoretical density-of-states calculated by Ciraci and Batra. The energy loss data have been used to determine the bulk plasmon energy of sapphire, 24.0 ± .3 eV, as well as the locations of eight regions of high conduction-band state density within 20 eV above the conduction-band minimum. One of these regions is an empty surface state 4.0 eV below the conduction-band minimum. Several high binding energy satellites in the XPS core level spectra are reported and interpreted in terms of energy losses to plasmons and interband transitions. Originator furnished keywords include:

See 1473 (Field 19)

I. INTRODUCTION

Aluminum oxide, Al_2O_3, in its various phases is important in a number of technological applications that include heterogeneous catalysts and microelectronic devices. In order to better appreciate the role of Al_2O_3 in these areas, a detailed understanding of the surface electronic structure of the different forms of Al_2O_3 is required. Previous experimental studies of Al_2O_3 used techniques such as optical absorption and reflection spectroscopies,[1-3] electron energy loss spectroscopy (ELS),[4-6] and photoconductivity[7] to determine the bulk electronic structure of Al_2O_3. These electronic structure studies were performed on samples ranging from single and polycrystalline α- and γ-Al_2O_3 to amorphous films. The main objective of the optical experiments was the determination of the band gap in the various forms of Al_2O_3. This determination was complicated by the possibility that an excitonic state existed near the conduction-band minimum (CBM).[3,8] In addition to the band gap information, the absorption data of Arakawa and Williams[3] contained some intriguing features which could not be attributed either to plasmons or to excitonic transitions. Earlier ELS data by Swanson[5] contained similar features, which are apparently the result of interband transitions in Al_2O_3.

Several theoretical determinations of the electronic structure of various Al_2O_3 analogues have been performed. These calculations were based on semiquantitative models,[9,10] or molecular units of the types AlO_4^{5-}, (Ref. 11) AlO_6^{-9}, (Refs. 12 and 21) and Al_2O_3 (Ref. 13). More sophisticated calculations used semiempirical techniques, such as the Mulliken-Rudenberg method,[14] or the extended tight binding

approximation.[15] The most recent calculation, which employed a modified extended Huckel Theory, is that of Ciraci and Batra,[16] who presented comparisons with good agreement between their theory and existing experimental data. They also presented the results of a calculation for a thin Al_2O_3 slab, which emphasized the surface contributions to the electronic structure.

The first attempt to establish the experimental Al_2O_3 band structure in the conduction, valence, and core regions was made by Balzarotti and Bianconi (BB).[17] They used X-ray photoelectron spectroscopy (XPS) on various forms of Al_2O_3, in conjunction with existing optical[3] and ELS data,[5] in order to establish the band structures of α-, γ-, and amorphous Al_2O_3. BB concluded that all three forms of Al_2O_3 had similar electronic structures. Especially noteworthy features were an excitonic state just below and a high density of states just above the CBM. XPS data for α-Al_2O_3, which differed slightly from that of BB, were also reported by Kowalczyk, et al.[18] The electronic structure of Al_2O_3 was also studied by X-ray absorption spectroscopy (XAS),[19-24] X-ray emission spectroscopy (XES),[23-26] and reflection ELS.[4,27,28] Reflection ELS can be performed with low energy electron beams to enhance the sensitivity to surface losses. The ELS experiments of Olivier and Poirier (OP)[28] contained features which were not observed in previous optical measurements. Extensive studies of oxygen chemisorbed on well defined Al surfaces have also been undertaken.[29] The X-ray absorption results from some of these studies have been extrapolated to Al_2O_3 surfaces.[30,31] However, these experiments were performed on samples grown from the <u>in situ</u> oxidation of

aluminium metal, the pyrolitic decomposition of $AlCl_3$, or amorphous Al_2O_3 samples which were sintered in air. Consequently, the phase composition of the samples in these studies was uncertain. In order to determine the bulk and surface electronic structure of the various phases of Al_2O_3, experiments should be performed on well characterized surfaces of single crystals.

The most well defined Al_2O_3 surfaces currently available are prepared from industrial sapphire (corundum), which is undoped, single crystal α-Al_2O_3.[32] High quality sapphire samples are commercially available, since several different crystal faces are often used as substrates for epitaxial growth of silicon-on-sapphire (SOS) structures. The sapphire $(1\bar{1}02)$ surface has been studied extensively by low energy electron diffraction (LEED), Auger electron spectroscopy (AES),[33-35] and Rutherford backscattering spectroscopy[36] in conjunction with SOS applications.

In order to initiate more careful studies of the electronic structure of the various forms of Al_2O_3, this study employed a combination of XPS and reflection ELS techniques to gather information from a single crystal of sapphire oriented to expose a $(1\bar{1}02)$ plane. The details of the experimental procedure used are discussed in Section II, and the results of the experiments are presented in Section III. The data are compared to the band structure calculations of Ciraci and Batra[16] in Section IV, along with a discussion of how the interpretation of the present results compares and contrasts with the work of other investigators. The primary conclusions of this study are listed in Section V.

II. EXPERIMENTAL PROCEDURE

Single crystals of sapphire oriented and polished on the $(1\bar{1}02)$ plane were obtained from the Union Carbide Company, Crystal Products Division. Using a diamond tipped scribe samples were cut to approximately 5x15 mm for the ELS studies and 5x5 mm for the XPS experiments.

A. XPS Measurements

The XPS measurements were performed with a UHV modified Hewlett Packard HP5950A electron spectrometer equipped with a monochromatized Al Kα (hν = 1486.6 eV) X-ray source. The Al_2O_3 crystal used for the XPS experiments was etched in HF for 2 minutes, rinsed in H_2O, blown dry with N_2, and mounted on a molybdenum plate with indium. The sample was then immediately loaded into the spectrometer vacuum system. The sample was heated in UHV ($5x10^{-9}$ Torr) for several minutes at 750 °C. This procedure produced a clean Al_2O_3 surface as determined by an XPS survey scan (0 - 1000 eV binding energy region). The only observed contamination was F (approximately 1/100 monolayer) residue from the chemical etch treatment. No LEED pattern was observed from this surface. High resolution spectra of the Al 2s, Al 2p, and O 1s core levels, as well as the O KVV Auger transition and the valence-band region were obtained. Al and O appeared to be in only one chemical state. No growth of O or C during the course of the measurements was observed by monitoring the O 1s and C 1s regions before and after the measurements.

B. ELS and AES Measurements

Prior to the ELS and AES experiments, the samples were ultrasonically cleaned in acetone and methanol and then dipped in a concentrated solution of HF for 30 seconds. Sample heating was accomplished by a method similar to that of Chang.[33] In this study, a sandwich was made by placing a 0.02-mm Ta sheet between two sapphire crystals and the set was securely tied together with two Ta wires. The sandwich was mounted by clamping excess Ta sheet, which extended from both ends of the sandwich, to the sample manipulator (Varian model 981-2523). The sample was heated by passing a current of up to 10 A through the Ta sheet. Approximate sample temperatures were measured by means of a Pt-Pt/10%Rh thermocouple that was spot welded to the Ta heater near the sapphire crystals. An optical pyrometer was used for the highest temperature range. Once under vacuum, the samples were cleaned by successive Ar^+ ion bombardment (typically 1.5kV at 20mA) and heating to approximately 1500 C. After the initial cleaning cycle, the samples were recleaned every day by heating only.

The ELS experiments were conducted in an ion pumped UHV chamber with a typical base pressure of $2x10^{-10}$ Torr. The chamber was equipped with a standard Varian LEED system which was used to determine the two dimensional order of the sample surface. AES and ELS were performed with a PHI single pass cylindrical mirror analyzer (CMA) and coaxial electron gun (PHI model 10-234G). The sample was always oriented perpendicular to the incident electron beam. For AES the instrument was run in $dN(E)/dE$ mode while $-d^2N(E)/dE^2$ mode was used for ELS.[37-39] A DEC LSI 11/23 minicomputer controlled the pass energy of the CMA. This computer control allowed accurate data collection over long counting times, precise assignment of

loss energies with respect to the incident electron energy, and the ability to numerically integrate the differentiated spectra that result from phase sensitive detection. An ELS sweep over 25 eV required from 5 to 30 minutes depending on the proximity of the sweep to the incident beam energy and the kinetic energy of the collected electrons. For a 150 eV incident electron beam, an effective modulation voltage of 1 V peak-to-peak resulted in an elastic peak with a 1 eV FWHM.

III. RESULTS

A. XPS: The Valence and Core States

The XPS valence-band spectrum of $(1\bar{1}02)$ sapphire is shown as the top curve in Fig. 1. Because of charging problems inherent in insulators, XPS data are commonly referenced to the valence-band maximum (VBM) or, if accurate optical data are available, to the CBM. In this paper, all XPS data are referenced to the CBM. The band gap is taken to be 8.5 eV, as suggested by OP.[28] The valence-band region is separated into two distinct bands, which will be called the upper valence-band (UVB) and the lower valence-band (LVB) after Ciraci and Batra.[16] The energy of the UVB maximum is determined from the XPS data by joining an extrapolation to the region of steepest descent in the valence-band electron distribution curve with a linear extrapolation of the baseline. The same procedure is used for the UVB minimum, except that the region of steepest descent is replaced by the region of steepest ascent. In this way, the width of the UVB is determined to be 9.7 eV. This method has been used previously for insulators[18] and gives good agreement with other methods.[17] The LVB region contains two intensity maxima, a major peak at 28.8 eV and a minor peak at 35.5 eV with

respect to the CBM. Because of the high sloping background, it is not possible to determine the positions of the energy minimum or maximum of the LVB very precisely, but the width of the LVB must be somewhat larger than the separation between the two peaks, 6.7 eV.

All of the accessible core lines, the Al 2p, Al 2s, and O 1s that are seen in Figs. 2 and 3, apparently consist of single lines and are assigned energies which correspond to the peak maxima. The energies for all of the observed occupied states are contained in Table I, along with values extracted from the XPS data of BB[17] with the present definition of the VBM. Examination of the XPS data in the regions behind the LVB, Al 2p, Al 2s, and O 1s core lines reveals a large number of satellites on the high binding energy side of the core lines. These satellites are labeled A through N in Figs. 2 and 3.

B. LEED and AES

Prior to the ELS experiments, the order and composition of the $(1\bar{1}02)$ sapphire surface were examined by LEED and AES. The AES data, shown in Fig. 4, were taken before any in-vacuum sample processing and after the sample was cleaned by Ar^+ bombardment and annealing. The Al LVV region of the AES data consists of three features at 35, 53, and 67 eV, while the signal due to O KVV Auger electrons is observed around 512 eV. Two features near 280 eV due to carbon, and perhaps also to calcium, contamination are also seen in the spectrum taken before cleaning. The spectrum taken after the sample was cleaned is representative of the sample surface both before and after ELS data were collected. The AES spectrum of

clean sapphire is very similar to that of sapphire before cleaning with the exception of the impurity peaks, which are absent from the clean surface. The observation that the Al LVV portion of the spectra does not change during the course of the ELS experiments indicates that the surface is not significantly damaged by the electron beam.

The LEED pattern of the clean and annealed sapphire surface revealed a a 2x1 reconstruction of the nearly four-fold symmetric $(1\bar{1}02)$ plane, which was previously observed by Chang.[34] The LEED pattern consisted of fairly sharp spots at beam energies down to about 90 eV. Below 90 eV, however, the LEED spots started to become diffuse and often faded away entirely after several minutes. The LEED and AES investigations showed that the surface was extremely clean, chemically stabile, and well ordered throughout the ELS data collection.

C. ELS: The Conduction-Band States and the Bulk Plasmon

ELS data were collected for $(1\bar{1}02)$ sapphire in five significant energy loss regions, which should correspond to the excitation of transitions from the various initial states to the conduction-band. Losses in the ELS spectra may also arise from the excitation of plasmons in the sample. The ELS spectra displayed in Figs. 5 through 9 correspond to possible interband transitions originating from the UVB, LVB, Al 2p, Al 2s, and O 1s states, respectively. There are 31 characteristic energy losses in these spectra that have been labeled a through ee. Although some of the energy loss features in the spectra appear to be weak, they were all very reproducible from day to day and from sample to sample. ELS spectra were collected at several different incident electron beam energies for each loss region, and spectra were also collected after varying amounts of electron beam dose to a particular spot on a sample. No variations occurred in the ELS spectra that could be attributed to electron beam damage to the samples, and the ELS spectra appeared to be unaffected by sample charging for incident beam energies of 150 eV or higher.

After the ELS experiments on clean sapphire were completed, nickel was evaporated onto the sapphire in amounts ranging from .5 to 5 equivalent monolayers, as monitored by a quartz crystal microbalance. In all cases, the addition of nickel resulted in severe surface charging, which did not allow a LEED pattern to be observed below incident beam energies of approximately 200 eV. The AES data also showed significant distortion from 0 to 200 eV. Analysis of the AES signal intensities versus the amount of nickel deposited indicated that the nickel formed islands on the surface

and did not cover the entire surface even when present in amounts equivalent to 5 monolayers. This experiment showed that metal impurities on the sapphire surface may act as charge traps, and that the surface must be extremely clean before meaningful results may be obtained with electron spectroscopic techniques.

D. XPS Satellites

A close examination of the XPS data displayed in Figs. 2 and 3 reveals several high binding energy satellites associated with each core level. It is very likely that these satellites are related to the energy losses observed in the ELS spectra. Figs. 11 and 12 have been constructed to show the relationship between the XPS satellites and ELS data. The ELS data is displayed as a function of N(E) rather than $-d^2N/dE^2$. This numerical double integration is possible because the data were collected digitally. Because of the complexity of Figs. 11 and 12, all features are referenced to the labels in Figs. 2 and 3. In Fig. 11, the O 1s XPS data are plotted with the O 1s core line as the zero of energy. From this point of view, all of the features in the electron distribution curve are a consequence of O 1s photoelectrons which lose energy. Fig. 12 is similar to Fig. 11 except that the satellites from both Al 2p and Al 2s photoelectrons are seen together. The upper energy scale and ELS data use Al 2s as the energy zero, while the lower energy scale and ELS are refered to Al 2p.

IV. DISCUSSION

A. XPS: Valence-Band Density of States

The XPS data were collected to obtain an accurate picture of the valence and core density of states in sapphire. The raw XPS valence-band data of Fig. 1a and the theoretical DOS shown in Fig. 1c, which was taken from the work of Ciraci and Batra,[16] are in qualitative agreement in that both have significant intensity in the same energy regions. The calculation has not been adjusted to agree with the experiment. However, there is a large difference between experimental and theoretical intensity ratios of the UVB to the LVB.

This discrepancy may be partly resolved if photoionization cross-section differences for the initial states of different orbital symmetry are considered. In order to obtain some quantitative correction to the ratio of the experimental UVB to LVB DOS, the cross-sections for the sapphire valence-band were approximated by the cross-sections for free O^{2-} subshells. The band structure calculations[16] show that the UVB and LVB are primarily O 2p and 2s in character, respectively. The Hartree-Slater calculations of Scofield[40] yield a ratio of 7.3 for the photoionization cross-sections of O 2s to O 2p for Al Kα excitation. The curve shown in Fig. 1b is the valence-band XPS spectrum after an arbitrary background has been subtracted and the integrated intensity of the LVB has been lowered by a factor of 7.3 with respect to the UVB. The resulting agreement between the ratio of the intensity under the UVB to that under the LVB between the modified experimental DOS and the theoretical band structure demonstrated in Fig. 1 is quite good. Further examination of the modified XPS data

reveal that the ratio of the UVB to LVB DOS is approximately 2.5 to 1. If O^{2-} was a perfect model for the sapphire valence-band, this ratio would be exactly 3 to 1. This level of agreement demonstrates that the corrected XPS data are reasonably self consistent. The major discrepancy between Figs. 1b and 1c is the relative intensity of the different features within the UVB, where the XPS data show two main features of nearly equal intensity, but the calculation contains one dominant peak with several smaller ones. This difference may be caused in part by the resolution function of the photoelectron spectrometer and by variations of the photoemission cross-section within the valence-bands, which do contain some Al character according to Ciraci and Batra's calculations.[16]

The XPS data presented in Figs. 1-3 and that of BB[17] are in general agreement, as demonstrated by Table I, but there are a few discrepancies between the two sets of data. Fig. 1 of BB shows three distinct features in the UVB region, while Fig. 1a provides no evidence of their highest binding energy feature. Older data by Kowalczyk, et al.,[18,41] on an Ar^+ bombarded surface are also missing this third feature, which is most likely the result of residual carbon contamination. In addition, BB attribute the asymmetry of the LVB feature to an unresolved plasmon satellite about 23 eV below the VBM. However, Fig. 1a shows two clearly resolved peaks in the LVB region. The theoretical DOS from Ref. 16 in Fig. 1c shows a broad LVB and a reasonably high DOS at a binding energy which corresponds to the minor peak in the experimental LVB. Thus, the minor peak in the LVB region of the XPS spectrum is caused by a transition from the appropriate initial state, rather than by an energy loss.

B. Sample Quality and Electron Beam Damage

In their ELS study of polycrystalline thin film α-Al_2O_3, OP[28] suggested that exposure to the primary electron beam dissociated Al_2O_3 to produce either metallic Al or reduced oxides of the form AlO_x on the sample surface. As evidence for this process, they note the presence of a peak at 67 eV in the Al LVV Auger spectrum, which was attributed to metallic Al. However, the Al LVV region of the AES data of this study (Fig. 4) is exactly the same before and after the electron beam exposures required to collect ELS spectra. Additional evidence for the possibility of Al_2O_3 surface modification as a result of extensive exposure to an electron beam is provided by the ELS spectra of Balzarotti, et al.[21] Initially, the spectrum for clean α-Al_2O_3 (Fig. 2 of Ref. 21) is very similar to those shown in Fig. 5 of this study. However, after 90 min. of exposure to a 300 eV electron beam of unspecified current, the ELS spectrum evolved until it resembled that of Al metal more than α-Al_2O_3. In the current study the ELS spectra do not change over a period of days or from sample to sample. Therefore, the electron beam is not damaging the sample in these experiments unless the damage is done during the first AES scan. The 67 eV AES feature in Fig. 4 could be the result of chemically different Al at or near the surface which is intrinsic to a clean sapphire $(1\bar{1}02)$ surface. Although the XPS data do not provide evidence for more than one chemically distinct Al species, electron mean-free-paths in sapphire indicate that the XPS sampling depth ranges from approximately 25 to 50 Å for O 1s and Al (2s, 2p) photoelectrons, whereas Auger electrons of about 50 eV sample only about 5 Å into the crystal.[42] Therefore, a distinct Al surface species

chemically shifted with respect to bulk Al may be seen by AES and not XPS. This may be seen clearly in the XPS spectra of Al metal with a thin oxide coating reported by Williams, et al.[43] In the usual sample geometry of the HP5950A spectrometer, the chemically shifted Al 2p peak was not observable, but was clearly evident when the sample geometry was changed to grazing electron collection angles to enhance the surface sensitivity. It is also possible that the surface species identified by the Auger spectra was not present at all on the surfaces analyzed by XPS, since the samples were prepared by slightly different methods.

C. Sapphire Plasmon

Using the simplest model for the volume plasma of an insulator,[44] the sapphire bulk plasmon energy may be calculated to be 25.5 eV assuming that only electrons in the UVB contribute to the plasma. The number density of electrons is estimated to be six times the density of oxygen atoms (ie. each O^{2-} ion contains 6 2p electrons), and the band gap of sapphire is 8.5 eV. Previous studies of sapphire and anodized aluminum by optical reflectance and absorption[2,3] and ELS[4-6,28] place the volume plasmon energy anywhere from 22 to 26 eV. In this study, peaks g, k, and m in the ELS spectra occur at 24.0, 48.6, and 71.6 eV loss energy, respectively, and have been assigned to one, two, and three quanta losses to the bulk plasmon. A least squares fit to these loss energies as a function of the number of quanta excited results in a volume plasmon energy of 24.0 $\pm$ .3 eV, in fair agreement with the above estimate. The present determination

should represent a reasonably accurate value for the q-averaged plasmon energy, since it is based on essentially three independent observations.

D. Interband Transitions and Surface States

The energy loss features that are not assigned to plasmon losses can be analyzed in terms of interband transitions. For a simple one electron model, in which any relaxation effects in photoemission transitions or excitonic effects in interband transitions are neglected, the interband transitions can be described as electronic excitations from bound states, either valence or core, to an unoccupied state in the conduction-band. The XPS data presented previously provide the energy position of the initial states. Consequently, the energy of final states can be determined in this one electron approximation by adding the energy of a loss feature due to an interband transition to the appropriate initial state energy. A set of one electron final states for sapphire was determined by using the method described above with the XPS and ELS data for the LVB, Al 2p, Al 2s, and O 1s. Only ELS peaks which may be assigned to final states that were accessed from at least three different initial states are considered here. The final state data, in conjunction with the energy loss data of Fig. 5, was then used to determine the initial states of the transitions which originate in the UVB. This procedure was used because the XPS data in Fig. 1a show that the UVB is very broad and does not have a single identifiable peak. The one-electron energy level diagram, which is consistent with both the core level and valence band data, is shown in Fig. 10. The 28 labeled interband transitions terminate at 8 well-defined final-state regions, which are listed in Table II. Assigning the UVB

maximum and minimum as the two possible initial states for the lowest energy loss features gives the best agreement with the final states determined from the core initial state energy loss features. The spectra are collected not as N(E) versus E but as $-d^2N/dE^2$, so that the sharp step functions present at the LVB minimum and maximum can yield peaks in the ELS spectra if the final state of the transition is narrow.

Balzarotti, et al.,[21] have made soft X-ray absorption measurements on thin Al_2O_3 samples which were made by sintering amorphous films in air. These samples were identified as α-Al_2O_3 with a background of the γ phase. Features in the X-ray absorption spectrum were assigned to electronic transitions between an Al 2p initial state and regions of the conduction-band. Energies of high state density in the conduction-band, which are consistent with the absorption spectrum (Fig. 3 of Ref. 21), are listed in the second column of Table II. In order to compare the ELS results from the current study with the X-ray absorption data a binding energy of 80.9 eV was assigned to the Al 2p level (Balzarotti, et al., used a value of 79.98 eV). Also, the energy of the excitonic peak, as measured from Fig. 3 of Ref. 21, was taken to be 79.5 rather than 78.9 eV, as listed in Table I of that paper, and feature A_5 was located at 91.0 rather than 90.0 eV. The agreement between the absorption and ELS data, which can be seen in Table II, is fairly good at energies of less than 10 eV above the CBM. Over 10 eV, the X-ray absorption data has a broad and intense absorption band, which is not seen in the ELS.

The most intriguing part of the energy level diagram (Fig. 10) is the state which occurs 4.0 eV below the CBM. Feature a at 4.7 eV loss energy

in Fig. 5 provides the best evidence for this energy level. Because the minimum energy of the band gap in sapphire is 8.5 eV, the interband transition corresponding to this feature must have an initial state in the valence-band and a final state at least 3.8 eV below the CBM. ELS transitions to this band gap state were also clearly seen for Al 2p (feature n) and O 1s (feature x) initial states (see Figs. 7 and 9). The spectra in Fig. 5 show that the relative intensity of feature a decreases with respect to the other features as a function of increasing electron kinetic energy. This behavior is exactly what would be expected if either the initial or final state of the interband transition were a surface state. Because core state ELS transitions to the same final state also show this dependence, the band gap state appears to be a surface state.

The ELS spectra for Al_2O_3 by Balzarotti, et al.,[21] have been discussed previously in regard to the surface modification by electron beam irradiation. It is important to reiterate that the spectrum of the undamaged surface of polycrystalline α-Al_2O_3 is virtually identical to those shown in Fig. 5 and a feature at approximately 5 eV loss energy is observed by Balzarotti et al., which is similar to feature a. This feature does not appear in the clean Al spectrum and does not change appreciably as the surface is reduced by electron beam exposure. If the feature at 5 eV loss energy is associated with a surface state, then the existence of this feature in the ELS of a polycrystalline sample and its invariance during the reductive removal of O from the surface indicate that the surface state is likely to be derived from Al dangling bond orbitals.

OP[28] used the results of their ELS experiments in conjunction with the XPS data of BB, XAS and XES data of Brytov and Romashchenko, and the optical data of Arakawa and Williams[3] in a manner similar to that described above to determine a high density of conduction-band states at -1.0, 1.0, 5.1, 9.8, and 19.5 eV with respect to the CBM. These states are in reasonable agreement with the present results, but several points should be noted in comparing the results of the two experiments. First, OP looked at thin polycrystalline films instead of a single crystal surface. Visual inspection of the ELS data presented in Figs. 2 through 4 of OP and that in Figs. 5 through 9 in this paper shows that the present spectra have significantly better resolution, and there is no reliable way to estimate the signal-to-noise ratio in the OP spectra because their figures appear to be hand drawn representations of their data. Also, OP reported three features at loss energies of 3.8, 4.2, and 5 eV, which they interpreted as indicating the presence of reduced Al produced by electron beam irradiation on their samples (they also observed features at 3.6, 4, and 5.2 eV on metallic aluminium). No evidence for electron beam reduction of the sapphire surface during ELS or AES measurements has been found in this study, but a great deal of care must be taken in assigning the low energy ELS features that have been observed.

The ultraviolet absorption spectra and spectrochemical analysis of sapphire crystals obtained from Union Carbide Corporation, similar to those used in our XPS and ELS experiments, have been reported by several groups.[45-47] These sapphire samples were found to contain less than 5 ppm each of common transition metal impurities including Fe, Ni, Cr, Co, Mn, V, and Ti, each of which has been found to produce absorption bands between 3

and 8 eV in sapphire.[48] In addition, the absorption spectra from as-received samples were essentially flat between 3 and 8 eV. However, exposure of such samples to high energy particle beams of neutrons or electrons,[45-47,49,50] or heating to 2000 C in a reducing atmosphere for 2h[46,51] resulted in the appearance of several absorption bands between 4.8 and 6.5 eV and one emission band at 3.8 eV. These bands are caused by the formation of F^+ and F centers, oxygen vacancies in the crystal which are filled by one or two electrons. An alternative explanation for the low energy ELS features observed by OP is that in generating their Al_2O_3 sample from the pyrolitic decomposition of $AlCl_3$ in a CO and H_2 atmosphere, a large number of defects were also formed in the crystallites. A set of experiments on Al_2O_3 samples grown under similar conditions to those employed by OP have found a series of trap states between 2.7 and 3.9 eV below the CBM,[52] which could account for the ELS features observed by OP.

The studies in which color centers were induced in sapphire by reduction heating or high energy particle bombardment indicate that the sapphire crystals used in this study were free of defects induced by sample preparation. The Auger and ELS data indicate that the sapphire was not damaged by electron irradiation unless extremely low beam doses permit the reduction and removal of O. Also, the temperature used to anneal the sample was not high enough, nor was it sustained long enough to create many O vacancies, since temperatures near 1800 C for 2 h in a reducing atmosphere did not create absorption bands in sapphire.[51] Consequently, the energy level 4 eV below the CBM is almost certainly an intrinsic surface state of sapphire ($1\bar{1}02$). The relative intensity of both the shoulder

labeled b in Fig. 5 and the -4 eV surface state decreases with respect to the remaining spectral features upon oxygen exposure. Since feature b is associated with a transition that has an energy level 1 eV below the CBM as a final state, this level may also be a surface state, although this energy region is also where the bulk exciton is found.

The results of a band structure calculation by Ciraci and Batra[16] for a slab of sapphire oriented along an Al terminated, unreconstructed (0001) face are shown in Fig. 10b. This calculation yields two empty band gap states, labeled S_p and S_d, which are approximately 1 and 5.3 eV below the CBM, respectively. Both of these states are derived mainly from surface layer Al broken-bond orbitals. Although the calculations were performed for a (0001) plane of sapphire and the experiments were performed on a $(1\bar{1}02)$ surface, the correspondence between theory and experiment suggests that both the experimentally observed band gap states are surface states due to an Al terminated $(1\bar{1}02)$ sapphire surface. The presence of Al with broken bonds at the surface was also suggested by the Auger spectra of Fig. 4, which indicate that the sample has two chemically different Al species near the surface. Soft X-ray absorption experiments of oxygen chemisorbed on Al single crystals suggest that the chemisorbed systems have two surface states approximately 2.5 and 3.5 eV below the excitonic feature.[30,31] However, because potentially large differences exist between the chemisorbed system and bulk α-Al_2O_3, as seen near the absorption threshold in Fig. 1 of Ref. 31, it is not possible to relate these features to the -4.0 eV surface state determined in the current study.

The surface state 4 eV below the CBM may be invoked to explain the relatively small amount of charging observed on clean sapphire surfaces.

Because the surface state is delocalized over the crystal surface, it may enable electrons impingent on the sample to flow rapidly away from the point of beam impact. However, impurities on the surface, such as nickel, may form localized trap states on the surface which could cause the large charging effects reported in the previous section.

All of the one electron transitions in the ELS spectra of sapphire have been interpreted in terms of excitations to regions of high state density in the conduction-band or in the band gap for the surface states. Heinrich, et al.,[53] reported ELS data on MgO (100) surfaces and interpreted the loss features in terms of transitions from the 2p and 2s states of Mg^{2+} to empty atomic orbitals of the dipositive ion. One set of transitions was primarily surface sensitive, and the remaining transitions were bulk derived. The surface states were interpreted as arising from atomic transitions of the surface Mg^{2+} ions which were energy shifted by a Stark field that was present at the surface of the ionic crystal. The energies of the bulk ELS transitions were in reasonable agreement with optical transitions for Mg^{2+} reported in Moore's Tables.[54] However, the energy level diagram of Fig. 10 shows that transitions to all but one of the various final states observed for sapphire occur from both O and Al initial states. This indicates that chemical bonding is important in the description of the final states of sapphire, in that they have both O and Al character, as shown by Ciraci and Batra in their band structure calculation.[16] However, the regions of high state density in the sapphire band undoubtedly arise from atomic-like states of the ionic species in the crystal, modified by chemical bonding. The data of Henrich, et al., may be

used to construct a one electron energy level diagram similar to Fig. 10 using the XPS data by Kowalczyk, et al.,[18,41] along with a 7.5 eV band gap derived from optical data.[55] The XPS data from Ref. 36 are summarized in Table I, and the conduction-band energy levels for MgO (100), which were derived by an analysis similar to that for sapphire, are shown in Table II. The most significant result is the surface state which lies 3.2 eV below the CBM of MgO. A slab calculation of the band structure of MgO (100) would be very useful in further analyzing the existing data sets for MgO.

E. <u>XPS Satellites</u>

The most prominent XPS satellites, labeled B, E, and L in Figs. 2 and 3, occur about 25 eV below the O 2s, Al 2p, Al 2s, and O 1s lines, respectively, and are undoubtedly due to energy loss from a photoelectron to a volume plasmon. Other strong features, labeled G and M, occur 50 eV below the Al 2s and O 1s lines and are due to double losses to the volume plasmon. The O 1s XPS data, Fig. 3, also contain a slight rise, labeled N, which may be caused by a triple volume plasmon loss. An additional strong satellite of the O 1s photopeak, labeled K in Fig. 3, is seen at approximately 13 eV below the core line. Fig. 11 shows that this XPS satellite has a corresponding ELS feature which has been identified as an interband transition.

The XPS data for the Al 2p and Al 2s energy levels also have satellites 13 eV below the core lines, labeled A and D in Fig. 2, which are due to the interband transition mentioned above. However, there are additional satellites labeled F and H through J in Fig. 2. A comparison of

ELS and XPS data in Fig. 12 leads to the assignment of feature F as an Al 2s photoelectron which loses energy to an interband transition between the LVB and conduction-band. A similar comparison for satellite H suggests that it may be due to losses from either an Al 2s photoelectron to an interband transition with an Al 2p initial state, or an Al 2p photoelectron exciting a transition with an Al 2s initial state. XPS satellites I and J could be due to similar processes, but the two XPS satellites correspond to only one ELS feature located at an energy intermediate to the two satellites. The absence of two features in this region of the ELS spectra may be due to the poor resolution of the CMA. The only completely unassigned satellite is that labeled C in Fig. 2, which may be due to a shake-up process.

XPS data for many other metal oxides can be found throughout the literature.[41] The spectra of MgO and TiO_2 contain satellite peaks behind several of the core lines. These satellites are very similar to those observed in sapphire, which indicates that the loss peaks observed in these metal oxides are also caused by plasmon losses and interband transitions excited by the photoelectrons.

V. Conclusions

These investigations have demonstrated that the $(1\bar{1}02)$ surface of sapphire can be prepared so that it is extremely clean and well ordered. The surface has a 2x1 LEED pattern and does not trap appreciable amounts of charge during electron bombardment by either LEED or AES electron guns. However, when even submonolayer amounts of nickel are deposited on the

surface, the sample charges up to as high as -350 V during electron bombardment.

An experimental, one electron energy level diagram has been constructed for sapphire from the data collected in this investigation and for MgO from literature data. The valence-band density of states of sapphire obtained from the XPS data, which has been corrected for cross-section effects, is in reasonable agreement with a band structure calculation by Ciraci and Batra.[16] The regions of high electronic state density in the conduction-band apparently arose from transitions to empty atomic-like orbitals of the constituent ions in the crystal. In addition, there is one empty surface state approximately 4 eV below the CBM of sapphire $(1\bar{1}02)$. This surface state reduces the effective band gap of the $(1\bar{1}02)$ sapphire surface from 8.5 to 4.5 eV. The state 1 eV below the CBM may be another surface state or an excitonic state. Finally, a series of satellites in the sapphire XPS data have been identified as energy losses to plasmons and interband transitions. XPS data for sapphire and other metal oxides have been in the literature for 10 years and the satellites have lacked a detailed explanation until now.

VI. ACKNOWLEDGMENTS

This work was supported in part by the Universitywide Energy Research Group (UERG) of the University of California and by the office of Naval Research. RSW acknowledges the Camille and Henry Dreyfus Foundation for a Teacher-Scholar Grant and the Alfred P. Sloan Foundation for a Fellowship. The authors thank I. Batra for his comments regarding this work and for supplying material incorporated into Figs. 1 and 10 of this paper.

REFERENCES

[1] G.H.C. Freeman, Brit. J. Appl. Phys. 16, 927 (1965).

[2] G. Stephan, J.C. Lemonnier, and S. Robin, J. Opt. Soc. Am. 57, 486 (1967).

[3] E.T. Arakawa and M.W. Williams, J. Phys. Chem. Solids 29, 735 (1968).

[4] C.J. Powell and J.B. Swan, Phys. Rev. 118, 640 (1960).

[5] N. Swanson, Phys. Rev. 165, 1067 (1968).

[6] L.B. Leder, Phys. Rev. 103, 1721 (1956).

[7] E.R. Il'mas and A.I. Kuznetsov, Sov. Phys.-Solit State. 14, 1255 (1972).

[8] E. Loh, Solid State Commun. 2, 269 (1964).

[9] M.H. Reilly, J. Phys. Chem. Solids 31, 1041 (1970).

[10] F.C. Douglas, Ph.D. thesis, University of Connecticut, 1970 (unpublished).

[11] J.A. Tossel, J. Am. Chem. Soc. 97, 4840 (1975).

[12] J.A. Tossel, J. Phys. Chem. Solids 36, 1273 (1975).

[13] K.L. Brower, J. Vac. Sci. and Technol. 12, 458 (1975).

[14] R.A. Evarestov, A.N. Ermoshkin, and V.A. Lovchikov, Phys. Stat. Sol. B 99, 387 (1980).

[15] I.P. Batra, J. Phys. C 15, 5399 (1982).

[16] S. Ciraci and I.P. Batra, Phys. Rev. B 28, 982 (1983).

[17] A. Balzarotti and A. Bianconi, Phys. Stat. Sol. B 76, 689 (1976).

[18] S.P. Kowalczyk, F.R. McFeely, L. Ley, V.T. Gritsyna, and D.A. Shirley, Solid State Commun. 23, 161, (1977).

[19] K. Codling and R.P. Madden, Phys. Rev. 167, 587 (1968).

[20] A. Balzarotti, A. Bianconi, E. Burattini, M. Grandolfo, R. Habel and M. Piacentini, Phys. Status Solidi 63, 77 (1974).

[21] A. Balzarotti, F. Antomangeli, R. Girlanda, and G. Martino, Phys. Rev. B 29, 5903 (1984).

[22] A. Balzarotti, F. Antomangeli, R. Girlanda, and G. Martino, Solid State Commun. 44, 275 (1982).

[23] V.A. Fomichev, Sov. Phys.-Solid State 8, 2312 (1967).

[24] I.A. Brytov and Y.N. Romashchenko, Sov. Phys.-Solid State 20, 384 (1978).

[25] C.G. Dodd and G.L. Glen, J. Appl. Phys. 39, 5377 (1968); J. Am. Ceramic Soc. 53, 322 (1970).

[26] D.W. Fischer, Adv. X-ray Anal. 13, 159 (1970).

[27] C. Benndorf, G. Keller, H. Seidel, and F. Thieme, Surf. Sci. 67, 589, (1977).

[28] J. Olivier and R. Poirier, Surf. Sci. 105, 347 (1981).

[29] I.P. Batra and L. Kleinman, J. Elect. Spect. 33, 175 (1984).

[30] A. Bianconi, R.Z. Bachrach, and S.A. Flodstrom, Phys. Rev. B 19, 3879 (1979); Solid State Commun. 24, 539 (1977).

[31] A. Bianconi, Surf. Sci. 89, 41 (1979).

[32] α-Al_2O_3, also known as corundum, has rhombohedral symmetry. However, it is usually refered to hexagonal axes for simplicity. See, for example R.W.G. Wyckoff, in 'Crystal Structures II', 2nd ed. (Wiley, New York,1964) or R. Nolder and I. Cadoff, Trans. Metall. Soc. AIME 233, 549(1965).

[33] C.C. Chang, J. Appl. Phys. 39, 5570 (1968).

[34] C.C. Chang, in 'The Structure and Chemistry of Solid Surfaces', ed. by G.A. Somorjai (Wiley, New York, 1969), article 77-1.

[35] C.C. Chang, J. Vac. Sci. Technol. 8, 500 (1971).

[36] J.C. Bean, Appl. Phys. Lett. 36, 741 (1980).

[37] For a discussion of ELS theory and experiment see H. Froitzheim, in 'Electronic Spectroscopy for Surface Analysis', ed. by H. Ibach (Springer, Berlin, 1977) p. 205.

[38] J.E. Rowe and H. Ibach, Phys. Rev. Lett. 31, 102 (1973).

[39] H. Ibach and J.E. Rowe, Phys. Rev. B 9, 1951 (1974).

[40] J.H. Scofield, J. Elect. Spec. 8, 129 (1976).

[41] S.P. Kowalczyk, Ph. D. Thesis, University of California, LBL Report LBL-4319 (1976) unpublished.

[42] M.P. Seah and W.A. Dench, Surf. and Inter. Anal. 1, 2 (1979).

[43] R.S. Williams, S.P. Kowalczyk, P.S. Wehner, G. Apai, J. Stohr, and D.A. Shirley, J. Electron Spectrosc. Relat. Phenom. 12, 477 (1977).

[44] H. Raether, in 'Excitation of Plasmons and Interband Transitions by Electrons', (Springer-Verlag, Berlin, 1980).

[45] B.D. Evans, H.D. Hendricks, F.D. Bazzarre, and J.M. Bunch, in 'Ion Implantation in Semiconductors', ed. by F. Chernow, J.A. Borders, and D.K. Brice (Plenum, New York, 1977) 265.

[46] K.H. Lee and J.H. Crawford, Jr., Phys. Rev. B 19, 3217 (1979).

[47] B.D. Evans and M. Stapelbroek, J. Nucl. Mater. 85 and 86, 497 (1979).

[48] H.H. Tippins, Phys. Rev. B 1, 126 (1970).

[49] P.W. Levy, Phys. Rev. 123, 1226 (1961).

[50] E.W.J. Mitchell, J.D. Rigden, and P.D. Towsend, Phil. Mag. 5, 1013 (1960).

[51] K.H. Lee and J.H. Crawford, Jr., Appl. Phys. Lett. 33, 273 (1978).

[52] E. Harari and B.S.H. Royce, Appl. Phys. Lett. 22, 106 (1973).

[53] V.E. Henrich, G. Dresselhaus, and H.J. Zeiger, Phys. Rev. Lett. 36, 158 (1976).

[54] C.E. Moore, 'Atomic Energy Levels', U.S. National Bureau of Standards Circular No. 467 (U.S. GPO, Washington, D.C., 1949), Vol. 1.

[55] W.H. Strehlow and E.L. Cook, J. Phys. Chem. Ref. Data 2, 163 (1973).

Table 1. XPS binding energies in sapphire and MgO.

XPS Feature	Sapphire This Work (eV)[a]	Sapphire Ref. 17 (eV)[a]	MgO Refs. 18 and 41 (eV)[a]
Upper Valence-Band			
Energy Maximum	8.5 ± .3	8.5 ± .3	7.5 ± .3
Peak 1	11.8	11.8	10.0
Peak 2	16.5	15.8	12.7
Energy Maximum	18.2		14.0
Lower Valence-Band			
Major Peak	28.8	29.3	26.3
Minor Peak	35.5		30.0
Mg 2p			54.5
Mg 2s			92.9
Al 2p	80.9	79.9	
Al 2s	126.0	124.9	
O 1s	538.6	537.0	

[a]All energies are referenced to the respective conduction-band minima. Band gaps of 8.5[28] and 7.5[54] eV are assumed for sapphire and MgO respectively.

Table II. Conduction-band energy levels for sapphire and MgO.

Sapphire ELS[a] (eV)	Sapphire X-ray Absorption[b] (eV)	MgO ELS[c] (eV)[a]
-4.0 ± .3		-3.2
-1.0 ± .2	-1.4	-.8
	1.1	1.5
2.3 ± .3	2.1	3.3
5.0 ± .4	4.3	3.5
6.9 ± .1	7.3	6.4
8.7 ± .3		11.4
	10.0	14.1
11.6 ± .5		15.7
	15.0	18.7
	17.1	20.0
20.6 ± 1.0	20.1	23.0

[a]All energies are referenced to the conduction-band minimum. For sapphire and MgO band gaps of 8.5 and 7.5 eV respectively were chosen.

[b]Conduction-band energy levels calculated from the X-ray absorption data of Balzarotti, et al.[21] To facilitate comparison of ELS and absorption data, a value of -80.9 eV was used for Al 2p binding energy rather than -79.98. All energies for features in the absorption spectrum were taken from Table I of Ref. 21 except for excitonic and A_5 features (assigned values of 79.5 and 91.0 eV, respectively), as measured from Fig. 3 of Ref. 21.

[c]Conduction-band values for MgO calculated from ELS data in Ref. 52 and XPS data in Refs. 18 and 41. No error estimates for the ELS data provided.

FIGURE CAPTIONS

FIG. 1. (a) Valence-band XPS data for $(1\bar{1}02)$ sapphire obtained with monochromatized Al Kα x-radiation. All XPS spectra presented in this paper are referenced to the conduction-band minimum. (b) XPS data shown in (a) after background subtraction and scaling in order to reduce the area under the LVB by a factor of 7.3 with respect to the area under the UVB, in accordance with the calculated photoionization cross sections for O 2s and O 2p subshells.[40] (c) The theoretical total density-of-states for sapphire from a band structure calculation by Ciraci and Batra.[16]

FIG. 2. XPS data for sapphire in the energy region near the Al 2p and 2s core levels. The lower curve shows the Al 2p and 2s core lines and the background on the same scale. The upper curve is an enlargement of the background and clearly shows XPS satellites which are labeled A through J.

FIG. 3. XPS data for sapphire including the O 1s and F 1s core lines. Fluorine is the only impurity detected by XPS. The upper trace is an enlargement of the energy range behind the O 1s line and contains satellites labeled K through N.

FIG. 4. Representative AES for $(1\bar{1}02)$ sapphire. The upper curve was taken before the sample was cleaned and contains a peak due to carbon contamination. The lower curve is typical for a clean sample. The spectral features of note are the minima between 35 and 70 eV due to Al LVV

processes and those near 512 eV from O KVV processes. Except for the carbon contamination, the spectra are identical before and after cleaning, and no changes were observed from the clean spectra with electron bombardment during these experiments.

FIG. 5. Negative second-derivative energy loss spectra, $-d^2N/dE^2$, as a function of loss energy for $(1\bar{1}02)$ sapphire. Peaks in this energy range must be due to plasmon losses or interband transitions between the valence- and conduction-bands. Spectra are shown for three different incident beam energies (E_p) to demonstrate the loss feature intensity dependence on electron kinetic energy. Features are labeled a through g. Note that feature a occurs at less than 5 eV; well below the sapphire band gap.

FIG. 6. Energy loss spectra for interband transitions with O 2s or lower valence-band initial states in sapphire. Features are labeled h through l and the energy position near feature k is the expected location of a double plasmon loss.

FIG. 7. Energy loss spectra for interband transitions with Al 2p initial states in sapphire. Incident beam energies of 250 and 300 eV show sharp features (m through t), while the features are smoothed out in the 1250 eV spectrum because of the poor resolution of the CMA at high electron kinetic energies. Feature m is the energy location expected for a triple bulk plasmon loss.

FIG. 8. Energy loss spectra for interband transitions with Al 2s initial states. The incident electron beam energies shown are 400 and 1250 eV. Although the features labeled u and w are weak, they appeared reproducibly in several different spectra at 1250 eV.

FIG. 9. Energy loss spectra for interband transitions with O 1s initial states. Low intensities at low incident beam energies forced the use of a 1250 eV incident beam energy spectrum where the CMA resolution is low. However, all the labeled features were reproducible.

FIG. 10. (a) The empirical one electron energy level diagram for $(1\bar{1}02)$ sapphire. Occupied state energies were extracted from the XPS data while the conduction-band energies were obtained by adding the loss energies from the ELS data to the initial state energies. Conduction-band states are shown as horizontal lines. ELS transitions are represented by arrows from the initial to final states with the arrow heads (triangles) centered on the final state energy. (b) A theoretical density-of-states from a band structure calculation by Ciraci and Batra[16] for a 16 layer slab of sapphire terminated at a (0001) surface. The percentage of Al character in the two band gap states is represented by the black shading.

FIG. 11. Comparison of the XPS satellites to the ELS data. (XPS) The XPS data for the O 1s core line plotted with the maximum of the O 1s line as the zero of energy. This emphasizes the assignment of XPS satellites as energy losses from O 1s photoelectrons. (ELS) N(E) electron energy loss

pectra, versus loss energy, for sapphire. Selected doubly differentiated oss spectra from Figs. 5 through 9 were numerically integrated and plotted s N(E) versus energy loss.

FIG. 12. The three parts of this figure allow the Al 2p and 2s satellites o be compared with ELS data. (XPS) The XPS data in the Al 2p and 2s egions are enlarged and plotted with the maximum of the Al 2p line as the ero of energy on the bottom scale and the Al 2s line as the zero of energy n the top scale. (ELS a) These curves are integrated energy loss spectra, imilar to Fig. 11, plotted with the Al 2s line as the zero of energy loss. ELS b) Integrated energy loss spectra plotted with the Al 2p line as the ero of energy loss.

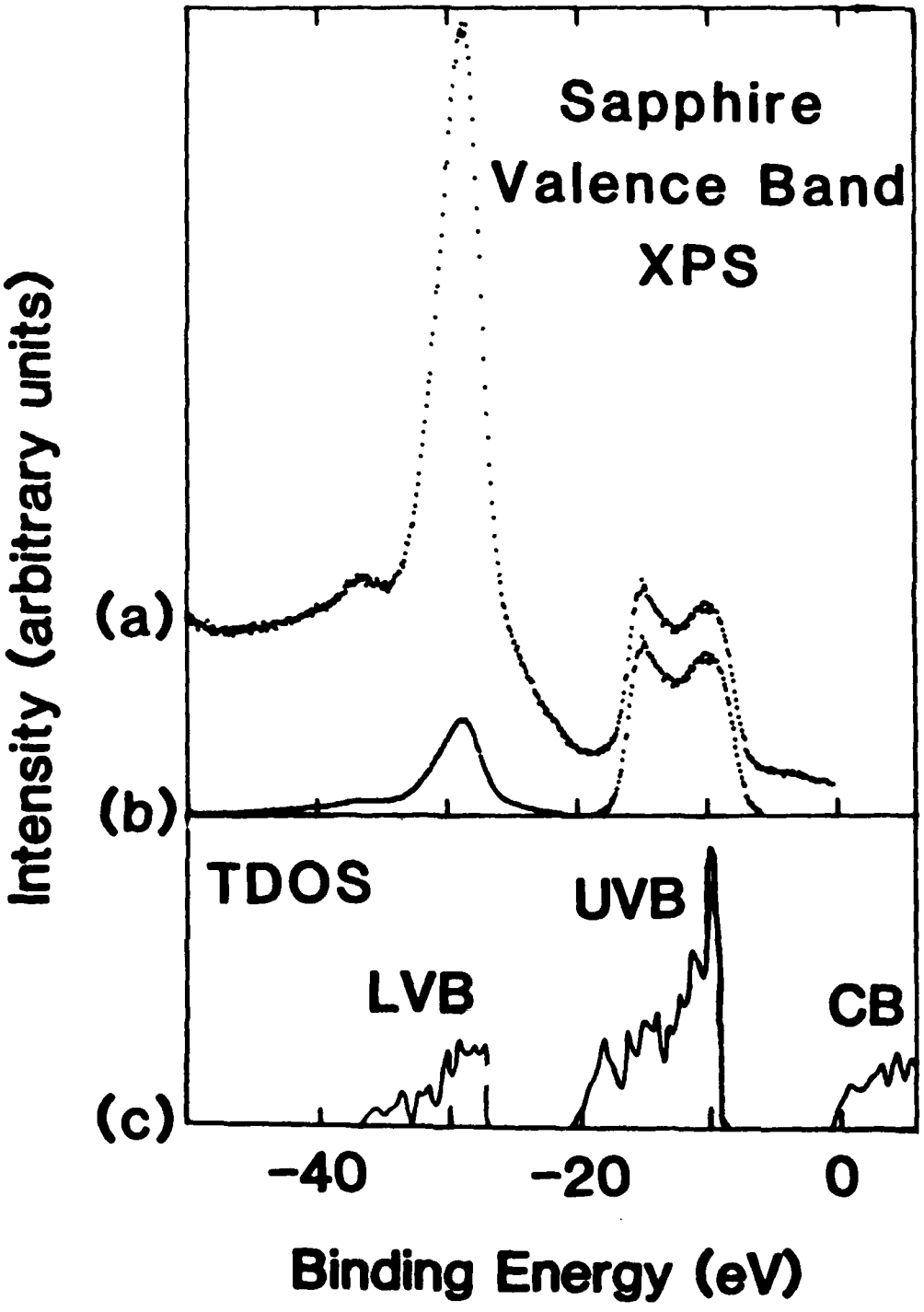
Sapphire
Valence Band
XPS
Intensity (arbitrary units)
(a)
(b)
(c)
TDOS
UVB
LVB
CB
-40
-20
0
Binding Energy (eV)

FIG. 1

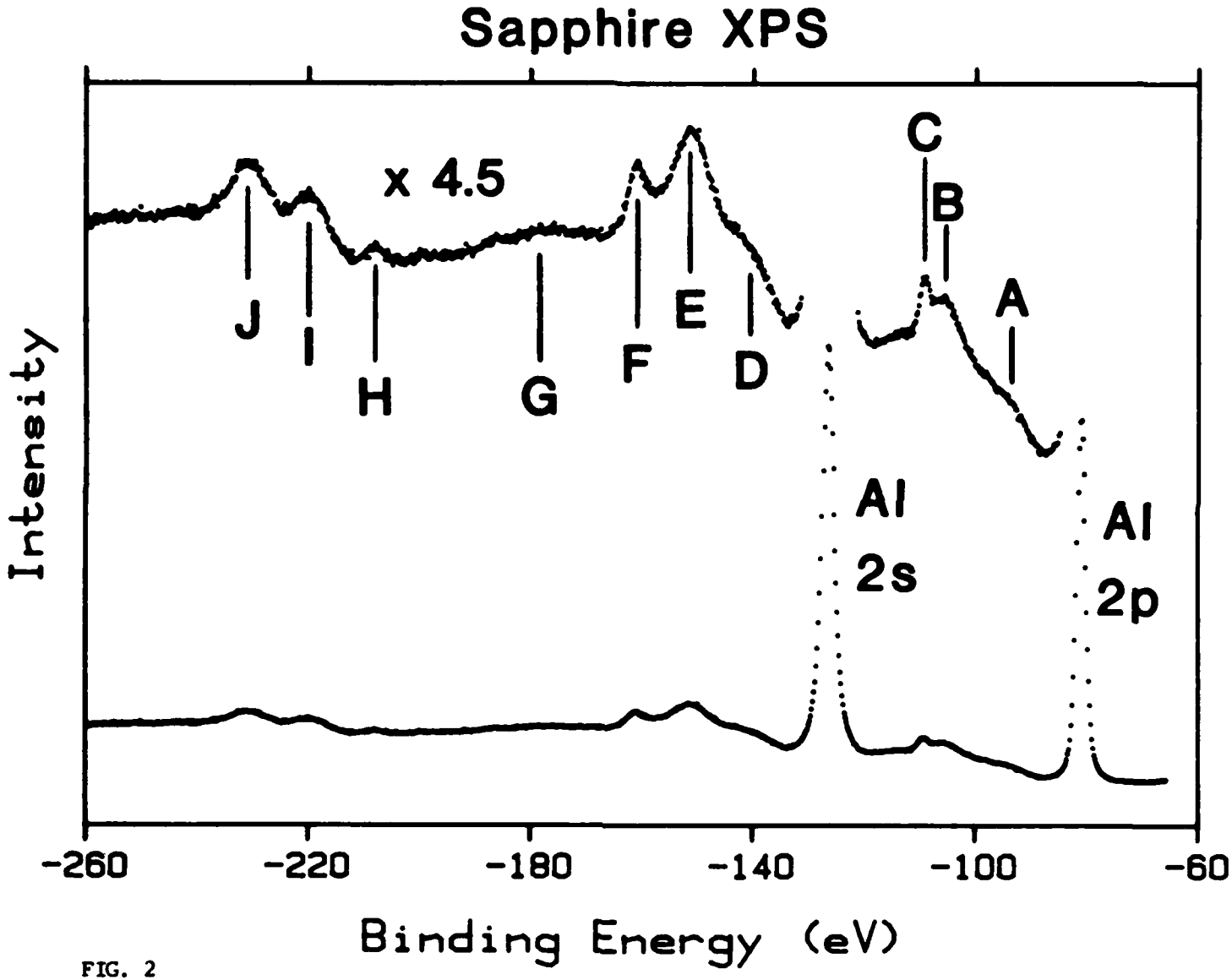
Sapphire XPS
x 4.5
J
I
H
G
F
E
D
C
B
A
Al
2s
Al
2p
Intensity
-260
-220
-180
-140
-100
-60
Binding Energy (eV)

FIG. 2

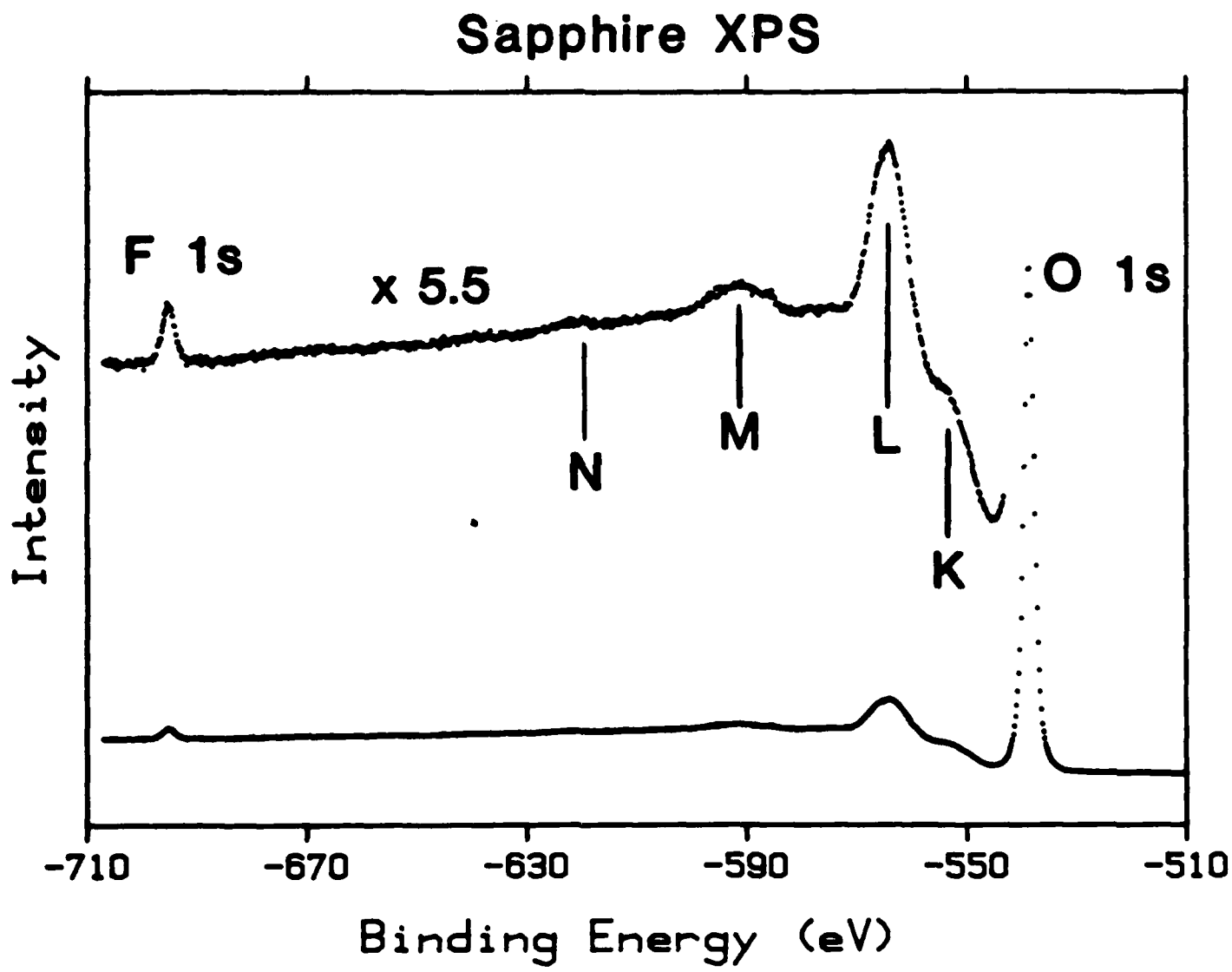
Sapphire XPS
F 1s
x 5.5
O 1s
N
M
L
K
Intensity
-710
-670
-630
-590
-550
-510
Binding Energy (eV)

FIG. 3

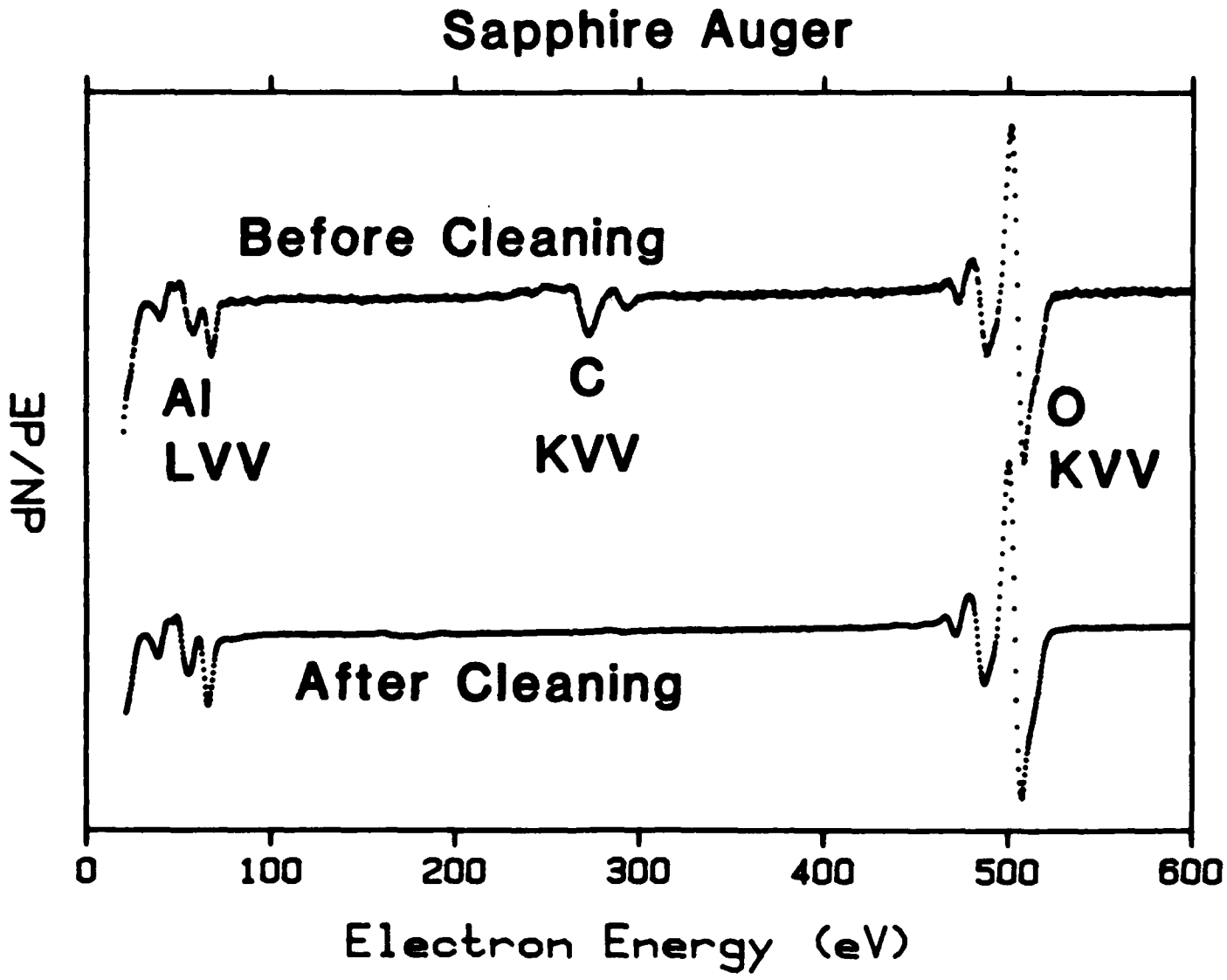
Sapphire Auger
Before Cleaning
After Cleaning
Al
LVV
C
KVV
O
KVV
dN/dE
0
100
200
300
400
500
600
Electron Energy (eV)

FIG. 4

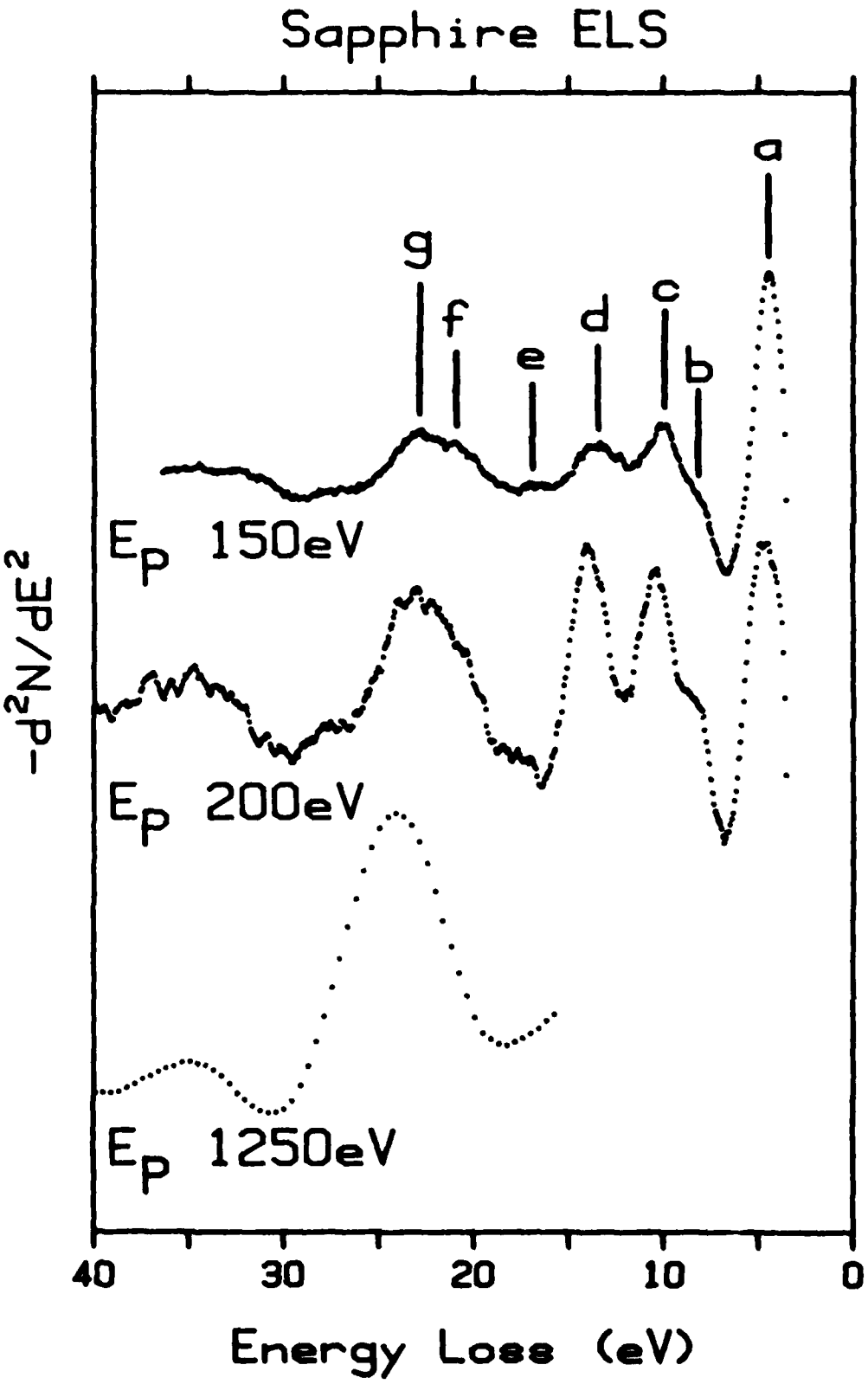
Sapphire ELS
a
g
f
e
d
c
b
E_p 150eV
E_p 200eV
E_p 1250eV
$-d^2N/dE^2$
40
30
20
10
0
Energy Loss (eV)

FIG. 5

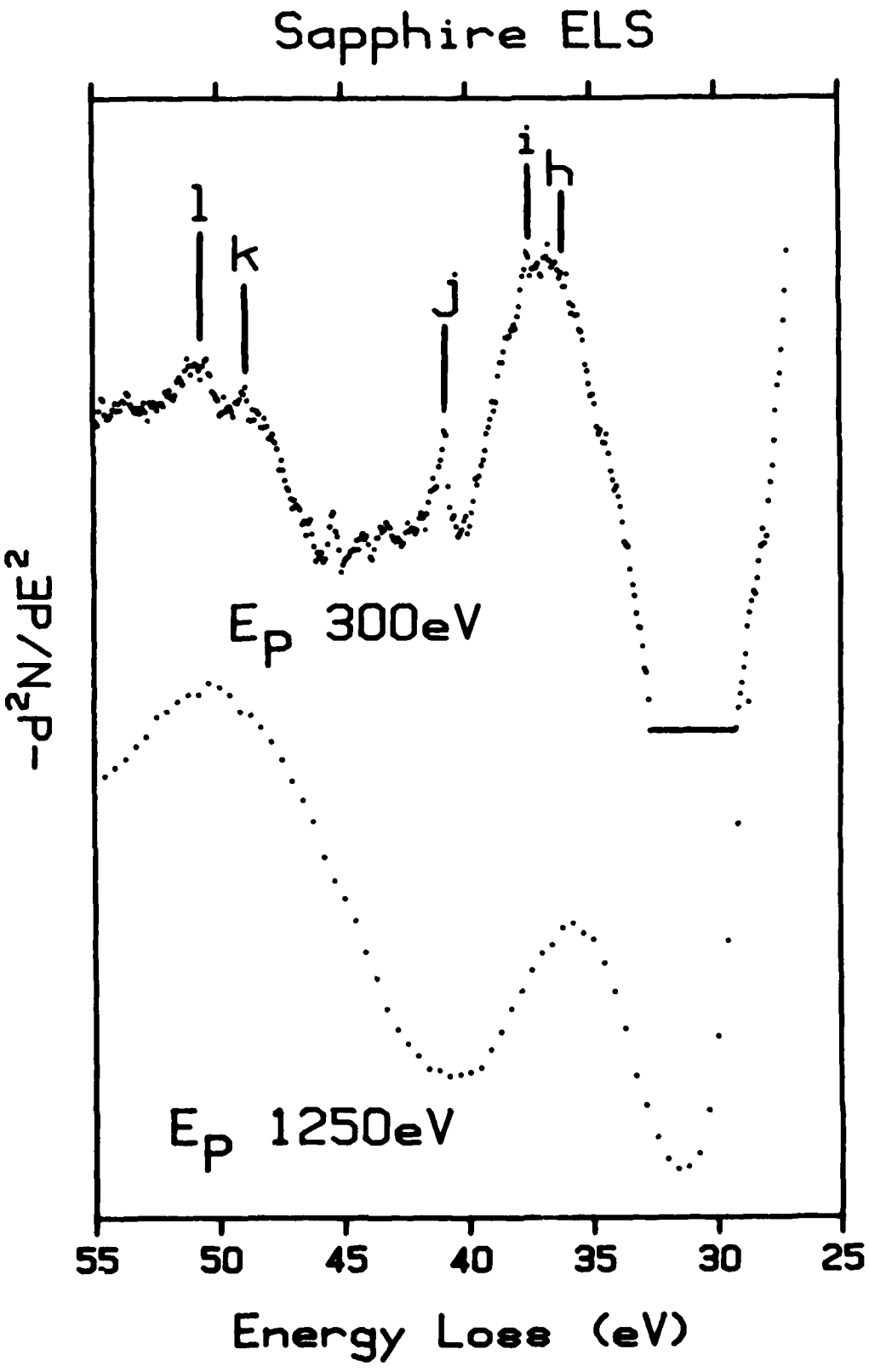
Sapphire ELS
l
k
j
i
h
E_p 300eV
E_p 1250eV
$-d^2N/dE^2$
55
50
45
40
35
30
25
Energy Loss (eV)

FIG. 6

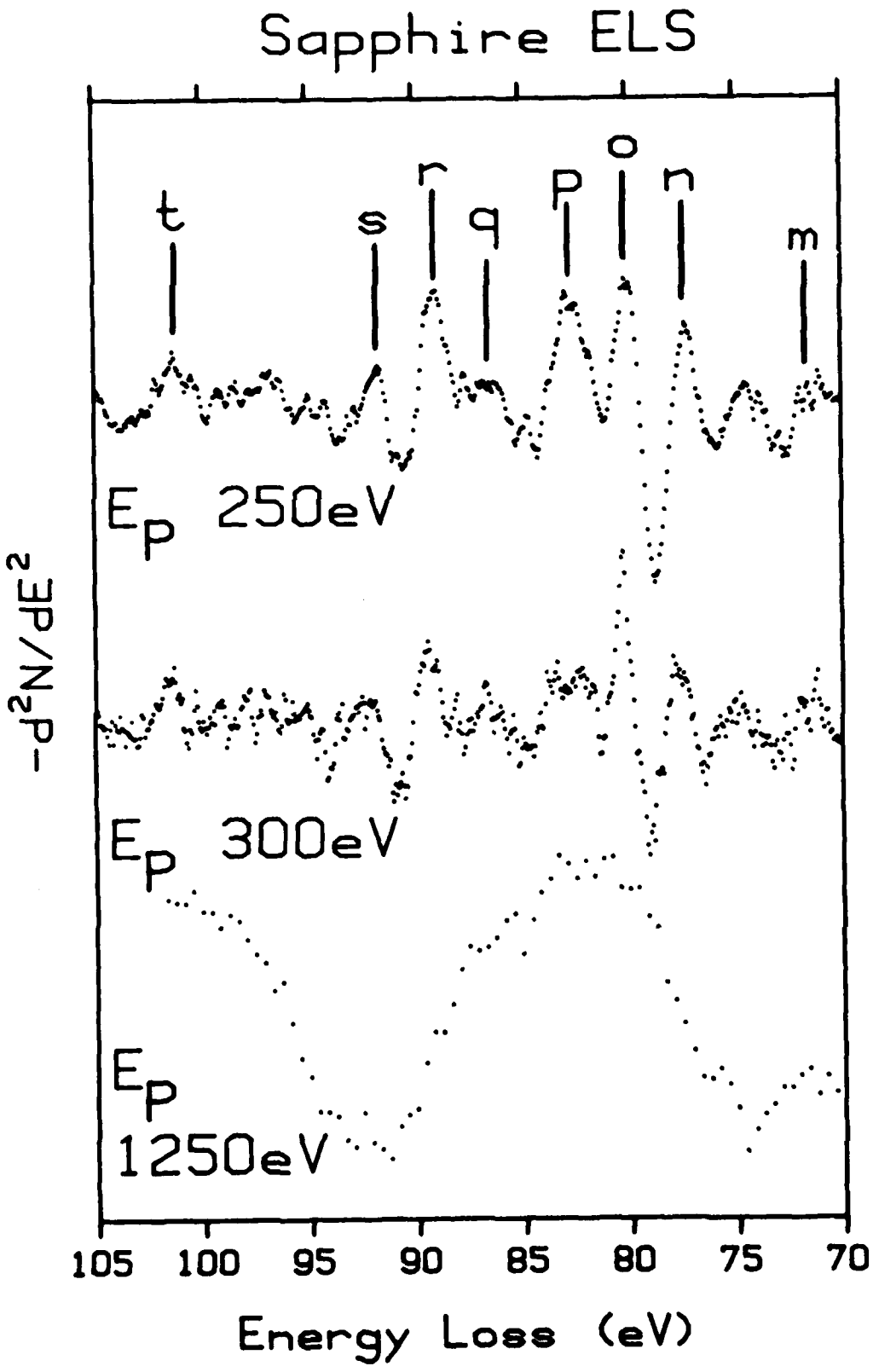
Sapphire ELS
t
s
r
q
p
o
n
m
E_p 250eV
E_p 300eV
E_p 1250eV
$-d^2N/dE^2$
105
100
95
90
85
80
75
70
Energy Loss (eV)

FIG. 7

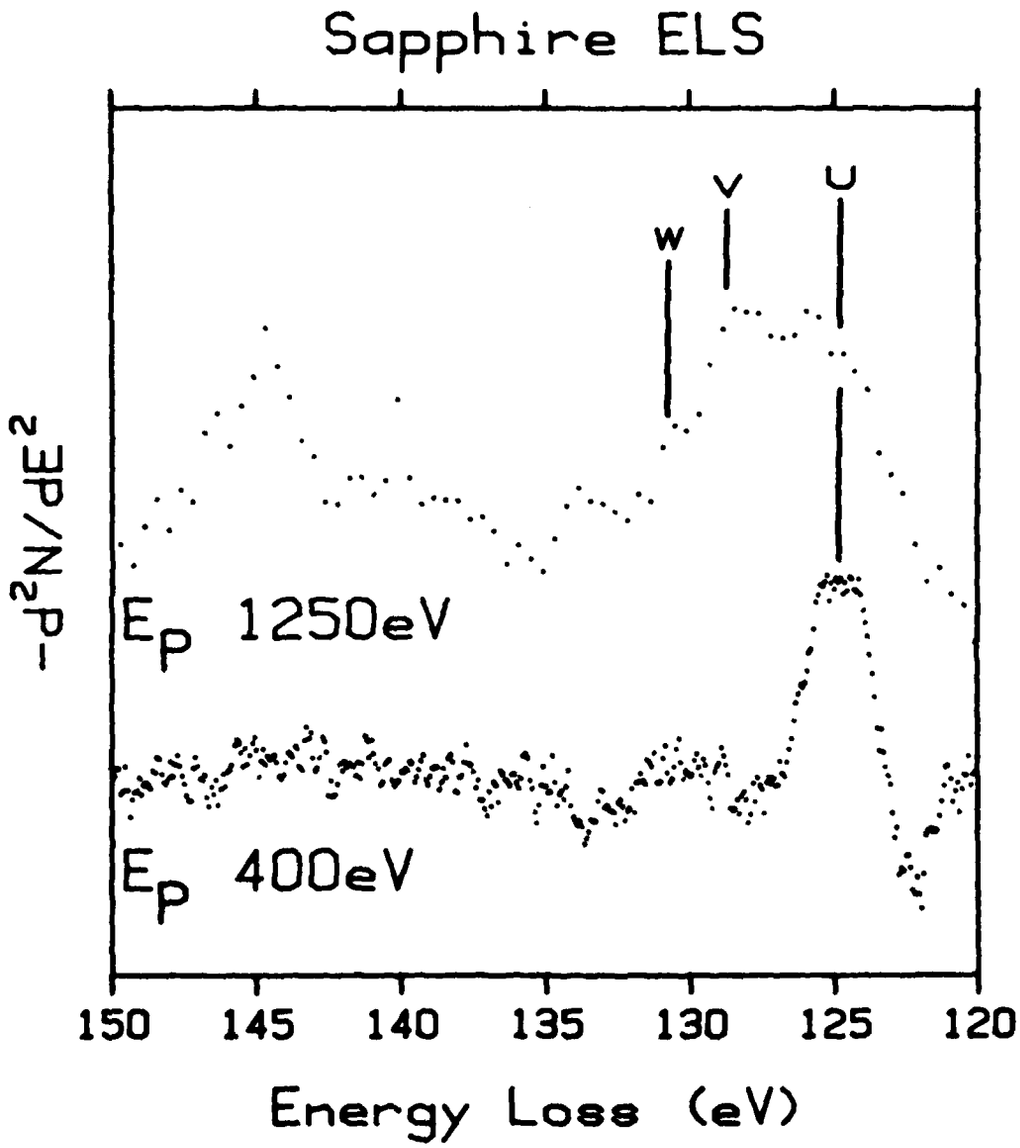
Sapphire ELS
W
V
U
$-d^2N/dE^2$
E_p 1250eV
E_p 400eV
150
145
140
135
130
125
120
Energy Loss (eV)

FIG. 8

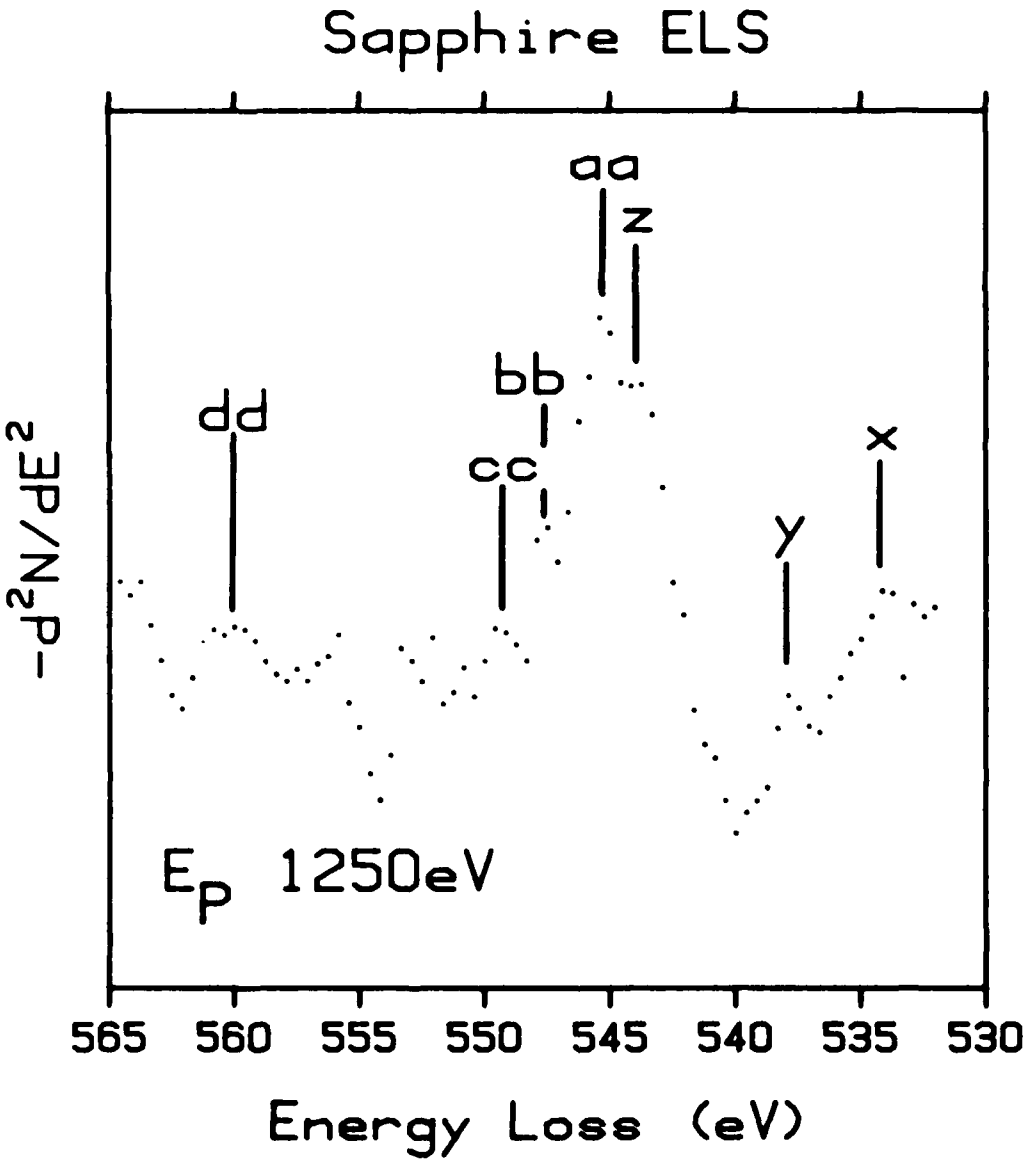
Sapphire ELS
aa
z
bb
dd
cc
x
y
$-d^2N/dE^2$
E_p 1250eV
565
560
555
550
545
540
535
530
Energy Loss (eV)

FIG. 9

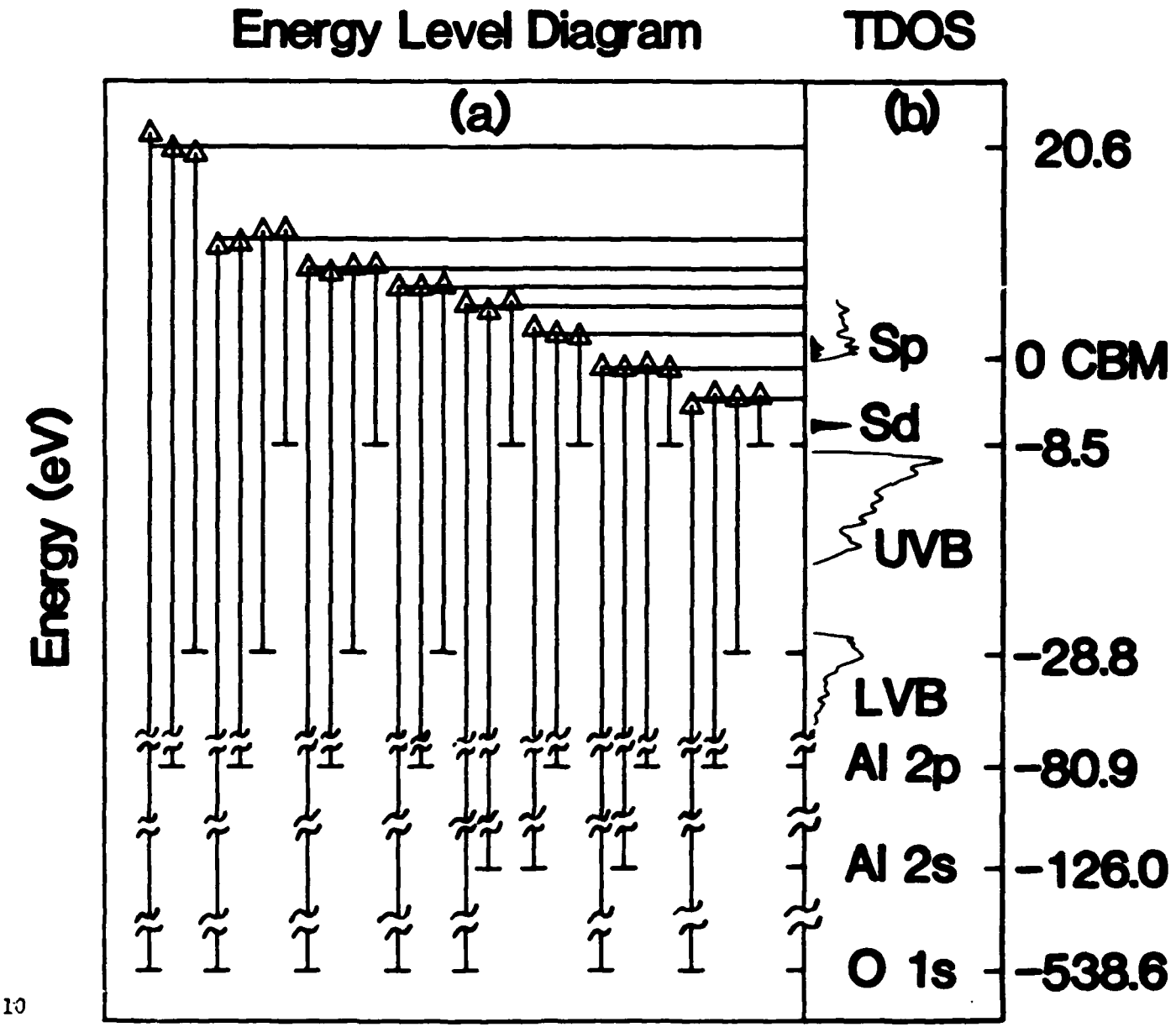
Energy Level Diagram
TDOS
(a)
(b)
Energy (eV)
20.6
0 CBM
-8.5
-28.8
-80.9
-126.0
-538.6
Sp
Sd
UVB
LVB
Al 2p
Al 2s
O 1s

FIG. 10

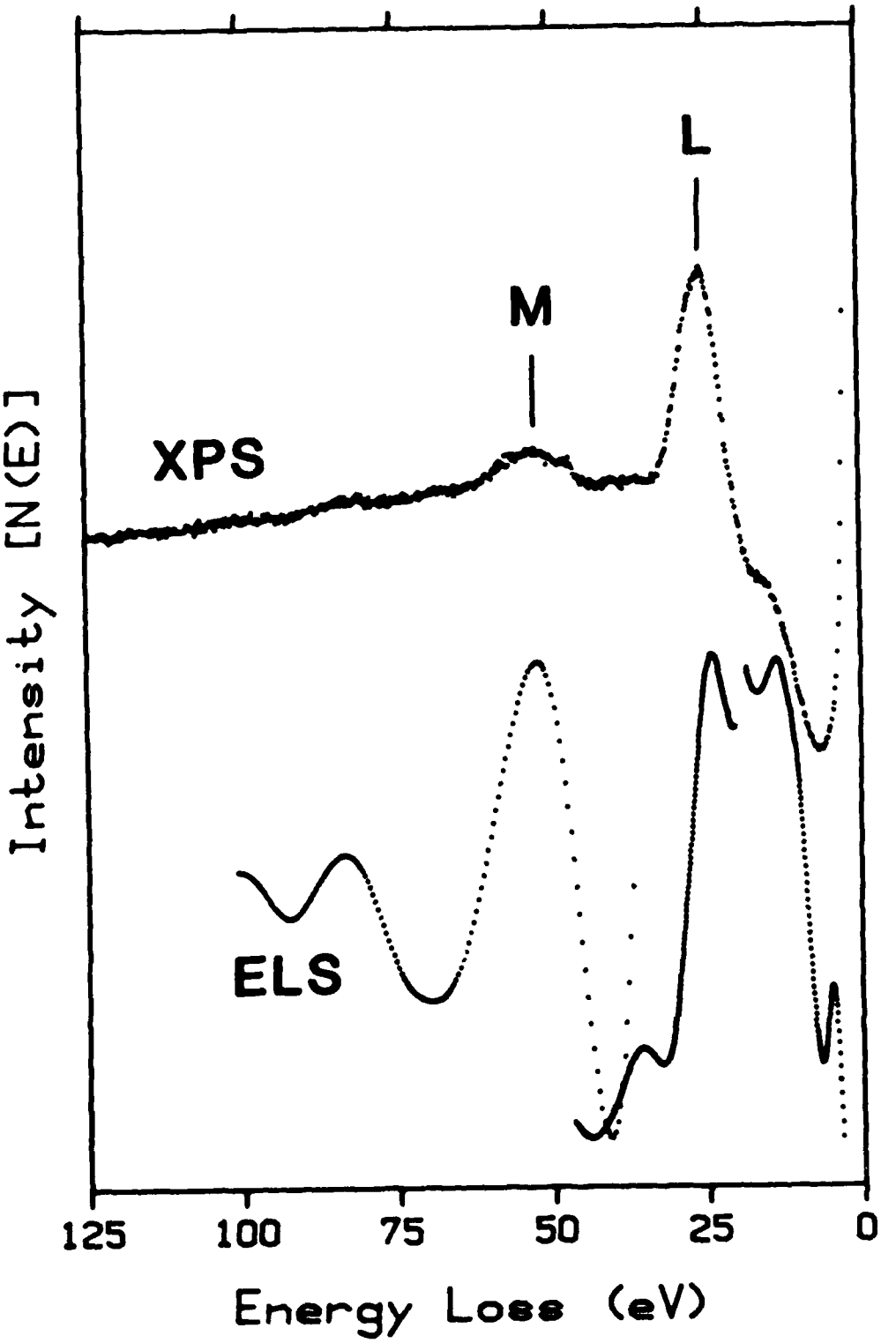

FIG. 11

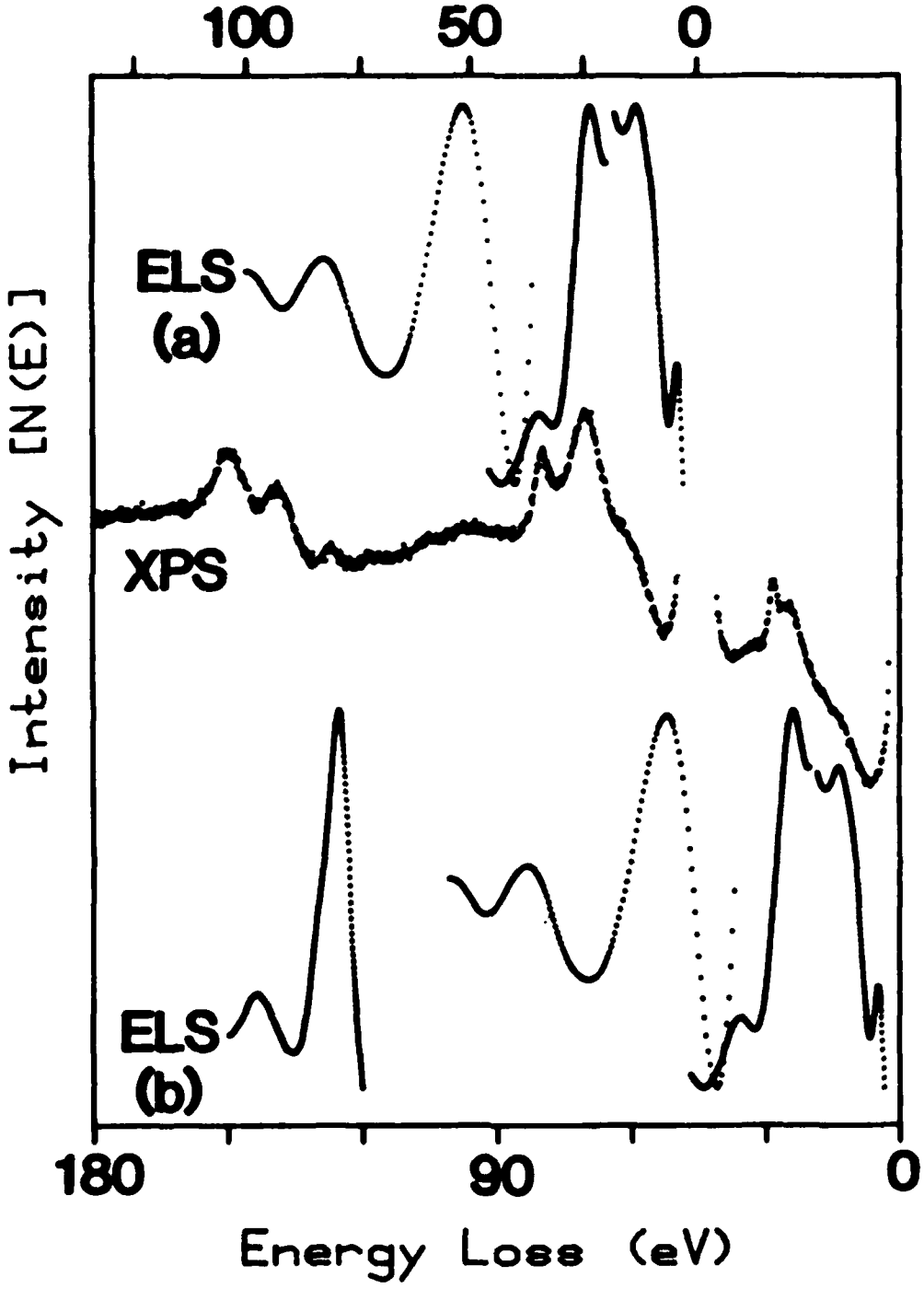

FIG. 12

LMED

-8